The x-ray light valve: A potentially low-cost, digital radiographic imaging system-concept and implementation considerations

Christie Ann Webster, Ivaylo Koprinarov, Stephen Germann, and J. A. Rowlands[a)]
Imaging Research, University of Toronto, Sunnybrook Health Sciences Centre, 2075 Bayview Avenue, Toronto, Ontario M4N 3M5, Canada

(Received 21 June 2007; revised 20 December 2007; accepted for publication 1 January 2008; published 19 February 2008)

New x-ray radiographic systems based on large-area flat-panel technology have revolutionized our capability to produce digital x-ray images. However, these imagers are extraordinarily expensive compared to the systems they are replacing. Hence, there is a need for a low-cost digital imaging system for general applications in radiology. A novel potentially low-cost radiographic imaging system based on established technologies is proposed—the X-Ray Light Valve (XLV). This is a potentially high-quality digital x-ray detector made of a photoconducting layer and a liquid-crystal cell, physically coupled in a sandwich structure. Upon exposure to x rays, charge is collected on the surface of the photoconductor. This causes a change in the optical properties of the liquid-crystal cell and a visible image is generated. Subsequently, it is digitized by a scanned optical imager. The image formation is based on controlled modulation of light from an external source. The operation and practical implementation of the XLV system are described. The potential performance of the complete system and issues related to sensitivity, spatial resolution, noise, and speed are discussed. The feasibility of clinical use of an XLV device based on amorphous selenium (*a*-Se) as the photoconductor and a reflective electrically controlled birefringence cell is analyzed. The results of our analysis indicate that the XLV can potentially be adapted to a wide variety of radiographic tasks. [DOI: 10.1118/1.2837288]

I. INTRODUCTION

In recent years, new x-ray radiographic systems based on large-area flat-panel technology have revolutionized our capability of producing digital x-ray images. These systems, called active matrix flat panel imagers[1] or AMFPIs, provide images very quickly. However, AMFPIs are extraordinarily expensive ($100,000–$200,000) compared to the systems they are replacing. This makes them unaffordable for all but a few selected procedures and institutions. Therefore, other approaches have been considered in the literature to make a low-cost x-ray imaging device for digital radiography.

One of the suggested approaches is to reduce the cost of existing flat-panel systems.[1,2] Flat-panel technology was originally developed using an indirect conversion approach. A major reason for developing the direct conversion AMFPI was that the fabrication method for the active matrix arrays could be made compatible with the standard *a*-Si:H TFT manufacturing processes used to make displays. Although this approach permits a lower cost than indirect conversion AMFPI, it cannot be regarded as a low-cost system.

A different method of producing a large imaging field is to create an image receptor that is essentially one dimensional and acquire the second dimension of the image by scanning the x-ray beam and detector across the patient.[3] A significant advantage of this approach is the excellent rejection of scattered radiation from the resulting image. However, this method has drawbacks: significantly increased mechanical complexity due to the requirement for an accurate system to synchronously scan the x-ray collimator and detector, and increased heat loading due to inefficient use of the output of the tube. These factors make the system cost comparable to that of AMFPIs.

Probably the most successful detectors for digital radiography to date have been photostimulable phosphors, also known as storage phosphors. Imaging plates made with photostimulable phosphors have been used in computed radiography (CR) systems with cassettes which are carried to a central processor for image readout. CR systems so far devised require two to four times as much radiation to achieve the same image quality (in terms of detective quantum efficiency) as AMFPIs.[4] The reason for this is the combination of the relatively poor x-ray absorption of CR screens having acceptable resolution and losses due to the secondary quantum sink[4] in the CR reader. It is possible to make somewhat higher image quality integrated CR systems by using structured phosphors, transparent phosphors, a double-sided readout, and/or linear scanning arrays but only with increased complexity and cost.[4] In summary, CR systems can achieve the image quality of AMFPIs only at higher exposures.

There have been various approaches to investigate readout systems based on photoconductors and particularly amorphous selenium (*a*-Se): 1. A digital method based on Xeroradiography was developed, which was read out using a scanning laser that stimulated an optical phosphor incorporated into the toner particles.[5] One major problem with this approach was that it was impossible to adequately remove the toner to reuse the plate; 2. In another method, the readout used an array of electrostatic probes held sufficiently close to the *a*-Se surface ($\sim$100 μm) to maintain adequate resolution.[6] This had the advantage of very low electronic

noise. Its only practical implementation used a drum coated with *a*-Se.[7] However, this approach failed because of its mechanical complexity and the high maintenance cost associated with the selenium drum and the microelectrometer replacement; 3. Methods based on optical discharge have also been attempted. They have the advantage of high resolution that is essentially limited by the precision of the focusing of the readout light onto the *a*-Se surface. There are, however, problems with noise sources not present in the electrometer readout method. The use of segmented readout electrodes or individual electrodes can reduce amplifier noise by lowering the capacitance loading of the preamplifier but no laser discharge method has yet been devised which eliminates the additional noise due to the bias charge that is read out in conjunction with the signal charge. As a result, all optical discharge methods have a poor signal to noise ratio.[8] In summary, all of the photoconductor based approaches discussed above have significant image quality problems and are expensive to make.

Optical coupling of a screen to a charge coupled device (CCD) (or complementary metal-oxide semiconductor) digital camera is the most intriguing approach in its basic simplicity—to combine a screen (a low cost, readily available item) with a scientific CCD camera. Unfortunately, despite many attempts to use this approach, it has been impossible so far to achieve a low-cost system with good image quality.[9] The physical reason is straightforward. It is difficult to make an optically coupled system with a significant demagnification without a serious secondary quantum sink. We can think of an indirect conversion AMFPI as the optimum limit of such a system. When the optical detector and the x-ray screen are of the same size, a good contact between the elements is possible, and by elimination of the lenses, essentially 100% optical coupling is achievable and with it, high detective quantum efficiency.

All these approaches are quite expensive and none have image quality matching that of AMFPIs. Therefore, a revolutionary approach to achieve a low-cost, high-quality digital x-ray system is needed. We have identified such an approach, the X-ray Light Valve (XLV).[10,11]

II. THE X-RAY LIGHT VALVE SYSTEM

The XLV incorporates several stages (x-ray absorption, image formation, and amplification) within a simple, compact structure with high resolution and potentially eliminates problems related to a secondary quantum sink. It combines three well-established, low-cost technologies: a photoconductor layer as the x-ray detector, a liquid-crystal (LC) cell used as an optically addressed spatial light modulator[12–14] and an optical imager. This arrangement allows the latent charge image created in the photoconductor layer by interaction with x rays to be made visible and stored in the LC cell, and subsequently to be digitized by the optical imager. This achieves our goal of immediate readout with an image quality comparable to that of an AMFPI while keeping costs very low. A related approach, using a polymer-dispersed liquid-crystal cell, has been considered for digital mammography.[15,16]

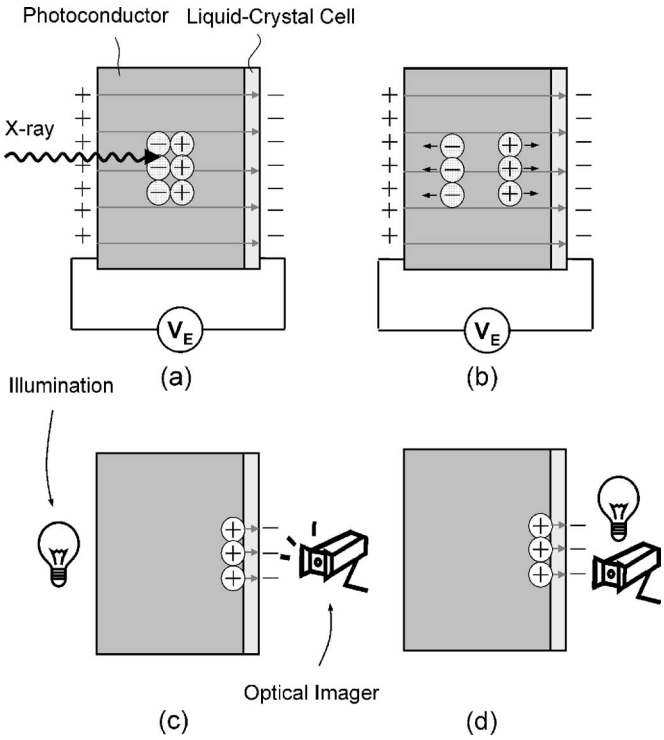

FIG. 1. Basic operation of the X-ray Light Valve. (a) X rays are absorbed in the photoconductive layer, generating electron-hole pairs within a localized region; (b) a large electric field due to the applied bias voltage V_E guides the electrons and holes to opposite surfaces of the photoconductor. After the exposure is finished and electric field is removed, the charge collected at the photoconductor-liquid-crystal interface remains there. The field created by the charge induces an optical image in the physically and electrostatically coupled liquid-crystal cell. The image is digitized using external illumination and an optical imager in a transmissive (c) or a reflective configuration (d).

The operation of the XLV system can be broken down into three steps: exposure, digitization, and reset. These will be briefly described to provide context for the more detailed discussion of the system design and properties which follows.

When an x ray is absorbed in the photoconductor, *electron-hole pairs* (ehp) are released [Fig. 1(a)]. A large applied electric field guides the electrons and holes to opposite surfaces of the photoconductor layer [Fig. 1(b)]. The charges follow the electric field, which ensures minimal lateral spread as the charges move. Thus, the charge image collected at the photoconductor-LC interface accurately reproduces the absorbed x-ray intensity pattern.

When the applied bias used to separate and guide the ehp is removed, the charges which have been collected and trapped at the interface remain there. The spatial variation of the field induced by the latent charge image across the LC layer modifies the molecular arrangement and controls the intensity of light passing through the LC cell. To summarize, variations in potential exist where the x rays were absorbed.

This causes spatial variations in the intensity of light passing the LC cell, allowing an optical representation of the x-ray absorption to be obtained.

The optical image is digitized using external illumination and an optical imager. This can be done in *transmissive mode*, with the readout light passing through both the photoconductor and the LC cell [Fig. 1(c)], provided that the photoconductor is transparent to the readout light. Alternatively, it may be done in *reflective mode* by having the illumination on the same side as the optical imager [Fig. 1(d)]. Optical coupling will not cause any image degradation as in the case of demagnified screen/camera systems because the XLV acts as an image intensifier whereby increasing the readout light intensity can compensate for any losses from the coupling optics. Therefore, the x-ray image can be recorded with an optical imager without a secondary quantum sink. It should be noted that the wavelength of the readout light is chosen such that it will not generate ehps and so erase the charge image at the photoconductor-LC interface. Such light is called *non-actinic*.

A key feature of the XLV is that the charge image is stored at the photoconductor-LC interface, allowing the digitization to continue over several seconds or even minutes if desired. As a result of this long storage time, it is necessary to reset the XLV, eliminating the latent charge image before a fresh exposure is made. To achieve this, the photoconductor is flooded with *actinic* light (i.e., of photon energy above the optical absorption edge of the photoconductor, thus creating free ehps). The charges produced will neutralize the image charge. The XLV is then ready to acquire a new image.

III. IMPLEMENTATION AND MATERIALS

III.A. Photoconductor

The photoconductor must have sufficient x-ray absorption, high sensitivity, high image resolution, and low dark current. At present the only practical material satisfying these requirements is *a*-Se. The clinical suitability of *a*-Se for medical x-ray imaging has been established previously in connection with Xeroradiography.[17] Currently, it is also used in direct conversion AMFPIs.[1] Large area *a*-Se detectors are feasible and cost effective since the photoconductor is amorphous and is made by evaporation techniques. They are easily scalable to the required size without increased complexity or excessive cost. The manufacturing process is well established because of its extensive past use in the photocopy industry.[18]

III.B. Liquid-crystal cell

The LC cell used in the XLV is similar to those used in common LC displays. LC technology is well established and inexpensive. Thus, LC cells can easily be made large enough to meet the size requirements[19] (35×43 cm) for general radiography.

LCs are organic molecules, which share some of the properties of liquids and some of those of solids. The molecules have short-range order similar to crystalline solids but lack long-range order; thus, the material can flow like a liquid. The molecules, generally elongated in shape, have anisotropic physical properties such as the dielectric constant and refractive index. Although several phases exist, the *nematic phase* is most widely used in display technology. It is characterized by a statistically preferred directional orientation without any positional order. Two parameters are used to describe the nematic phase: the *director*, which points in the microscopic preferred direction of the LC molecules, and the *order parameter*, which describes the distribution of the orientation of the molecules around the director. The combination of liquid behavior and the optical and dielectric anisotropy is fundamental for display applications. They permit the molecular orientation to be manipulated by a relatively modest electric field and so affect the light propagation. Almost all LC displays use *LC mixtures*[20] since there is no single LC material which could fulfill the specifications of even the simplest display.

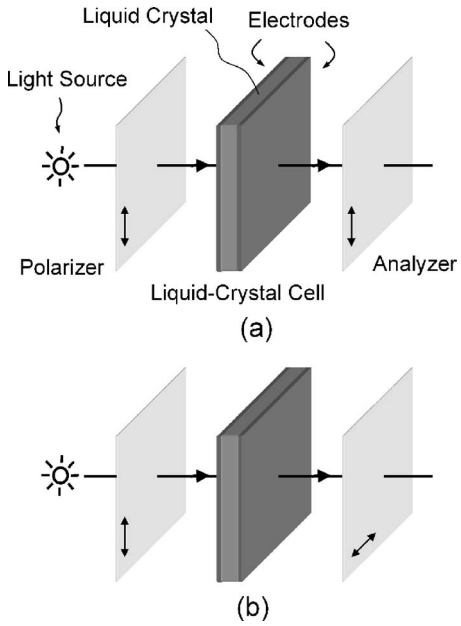

FIG. 2. The liquid-crystal cell consists of a layer of LC molecules aligned between two transparent electrodes, which are placed between two polarizers. The polarization axes (indicated by arrows) of which can be parallel (a) or perpendicular to each other (b). The input and output polarizers are known as the polarizer and the analyzer, respectively.

LC cells consist of a layer of LC molecules aligned between two transparent electrodes and two polarizers referred as the *polarizer* and the *analyzer*, the polarization axes of which can be parallel [Fig. 2(a)] or perpendicular to each other [Fig. 2(b)]—these are known as *parallel* and *crossed-polarizer configurations*, respectively. The surfaces in contact with the LC material are treated to align the LC molecules in a particular direction. This treatment typically consists of adding a thin polymer layer, i.e., *alignment layer*, which is then mechanically rubbed or photopolymerized in one direction that then defines the alignment of the LC molecules. In the absence of an applied electric field, the orientation of the LC molecules is determined solely by the align-

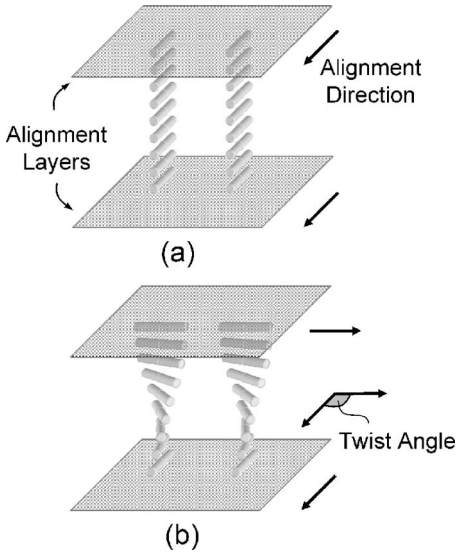

FIG. 3. The orientation of the liquid-crystal molecules is determined by the alignment at the surface of the alignment layers. If the alignments at the top and bottom are parallel (a), the molecules will be forced to align parallel throughout the liquid crystal layer. In the non-parallel case (b), the molecules closest to each surface are parallel to the alignment direction and gradually move throughout the layer so as to arrange themselves in a helical structure, or twist, described as a twist angle.

ment at the surfaces. If the alignment of the top and bottom are parallel, the molecules will be forced to align parallel throughout the LC layer [Fig. 3(a)]. In the non-parallel case, the molecules closest to each surface are parallel to the alignment direction and gradually move throughout the layer so as to arrange themselves in a helical structure, or *twist*, described as a *twist angle* [Fig. 3(b)]. When a potential is applied to the electrodes, a torque acts to align the LC molecules parallel to the electric field and distorts the original arrangement by tilting the molecules towards the electric-field direction (Fig. 4). This torque is resisted by elastic forces since the molecules are constrained at the surfaces. The *dielectric anisotropy* ($\Delta\varepsilon$), defined as the difference between the *dielectric constant parallel to the director*, $\varepsilon_{\parallel}$, and the *dielectric constant perpendicular to the director*; $\varepsilon_{\perp}$, determines how easily the molecule will rotate under the influence of the electric field. Alignment layers also provide a small specific *pre-tilt* in one direction to induce a preferred tilt direction when the electric field is applied (Fig. 5), which helps to prevent formation of domains with different tilts.

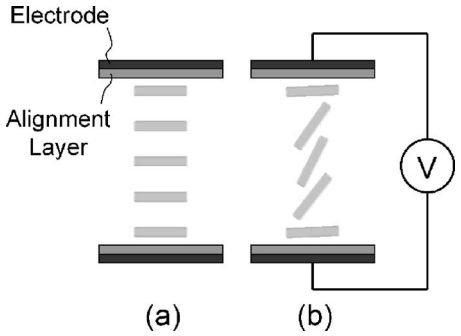

FIG. 4. A potential applied to the electrodes of the liquid-crystal cell distorts the original arrangement of the molecules in the liquid-crystal layer by tilting them towards the electric-field direction. The sketch shows a side view of a parallel alignment without (a) and with an applied potential (b).

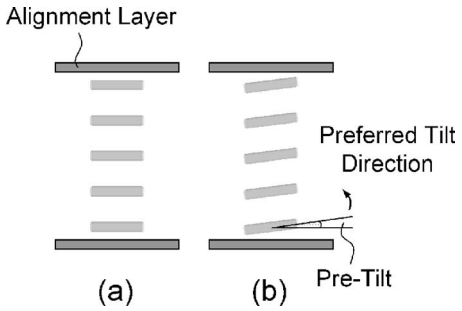

FIG. 5. Some alignment layers also provide a small pre-tilt. The pre-tilt induces a preferred tilt direction when the electric field is applied, which helps to prevent formation of domains with different tilts. The sketch shows a side view of a parallel alignment without (a) and with a small pre-tilt (b).

The optical anisotropy (known as *birefringence*) of the LC molecules is described by two indices of refraction, *extraordinary*, n_e, and *ordinary*, n_o, and defined as $\Delta n = n_e - n_o$. By using this property, the LC layer can be designed to rotate the polarization direction of linearly polarized light by 90°. Consequently, before applying an electric field, the linearly polarized light (after passing through the polarizer) is rotated by 90° as it passes through the LC layer. When operated in a crossed-polarizer configuration, this light will pass through the analyzer, making the cell appear transparent (known as *bright state*). If enough voltage is applied across the electrodes, the LC molecules will align with the field and the rotation of light polarization is eliminated. The light will then be polarized perpendicular to the analyzer and thus be completely blocked, causing the cell to block light transmission (*dark state*). By controlling the potential across the LC layer and hence modifying the effective anisotropy of the medium, light can be allowed to pass through in varying amounts to create shades of gray. However, a *threshold voltage*, V_{th}, needs to be exceeded before any optical activity is observed. It can be shown that, for a pre-tilt angle of zero, V_{th} depends only on the elastic constants and the dielectric anisotropy[24] of the LC. The LC cell can also be operated in a parallel-polarizer configuration, in which case, the bright and dark states are reversed.

Several physical mechanisms have been developed to modulate the polarization state of light by using LCs. These include the *polarization rotation effect*,[21] the *phase retardation effect* [also known as *electrically controlled birefringence*[22] (ECB)], and the *mixed mode*[23] (combined polarization rotation and phase retardation effects).

The *90° Twisted Nematic cell, or 90°-TN cell* is the most common LC display and uses the *polarization rotation effect*. The surface alignment directions at the two electrodes are perpendicular and, therefore, the molecules twist from one substrate to the other by 90° [see Fig. 3(b)]. An important parameter in such a helically oriented birefringent medium is the *Mauguin limit*, defined as

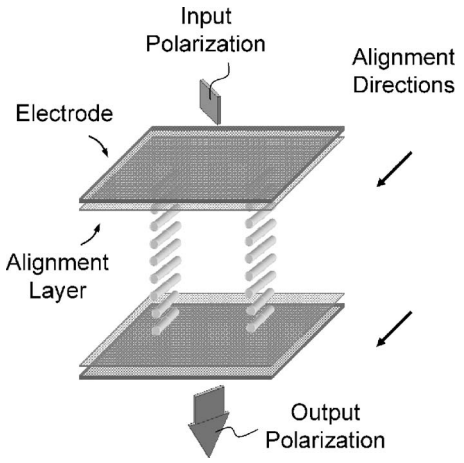

FIG. 6. The ECB cell is based on the phase retardation effect. Its alignment has the LC molecules aligned parallel. In the absence of an electric field, it acts as a half-wave retarder. To rotate the plane of polarization of linearly polarized light by 90°, the input polarization has to be oriented 45° to the director of the LC.

$$d\Delta n \gg \psi\lambda/\pi, \tag{1}$$

where Δn is the birefringence of the LC, d is the thickness of the LC layer or *cell gap*, ψ is the twist angle, and λ is the wavelength of the light. In the Mauguin limit, linearly polarized light follows the helical structure, also known as *wave guiding*. To fulfill this condition, twisted nematic devices generally require a certain value for the product of the cell gap d and the birefringence Δn of the LC mixture, which is optimized by considering parameters such as the twist angle ψ, the wavelength of the light λ, and the expected optical performance.[24] When the LC molecules begin to tilt due an applied voltage ($V > V_{th}$), the effective birefringence is reduced and the light which passes through the LC layer is generally elliptically polarized. In the high voltage regime ($V \gg V_{th}$), the helical structure is completely destroyed and the rotation of light polarization is eliminated.

The ECB cell is based on the *phase retardation effect*. Its alignment has the LC molecules aligned parallel (there is no twist) as shown in Fig. 6. The cell acts as a variably birefringent sheet where the retardation can be controlled by an applied electric field. Due to the different propagation velocities of the extraordinary and ordinary rays inside the LC, the slow component of the beam after passing through the LC layer will experience a phase retardation δ with respect to the fast component. The phase retardation is given by the following equation:

$$\delta = 2\pi d\Delta n/\lambda, \tag{2}$$

where d is the cell gap, Δn is the birefringence, and λ is the wavelength. The value of d is chosen such that, when $V=0$, the phase difference between the extraordinary and ordinary rays is exactly one-half cycle (also known as *half-wave retarder*). To rotate the plane of polarization of linearly polarized light by 90°, the input polarizer must be oriented 45° to the director of the LC (see Fig. 6). When $V > V_{th}$, the LC molecules begin to reorient with alignment in the direction of the electric field. As a result, the effective birefringence (and in turn the phase retardation) decreases and the light which passes through the LC layer is generally elliptically polarized. In the high voltage regime ($V \gg V_{th}$) virtually all LC molecules in the bulk are aligned with the electric field (i.e., normal to the substrates) and the rotation of light polarization is eliminated.

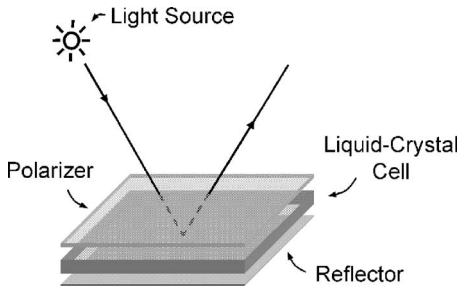

FIG. 7. In a reflective configuration, light from a lamp is reflected by a reflector built into the display. The reflective cell uses only a single polarizer, which acts as in the parallel-polarizer configuration, as incident light after reflection passes through it again.

Since the LC is a modulator of light and not an emitter, a light source is required to illuminate the device. In a *reflective configuration*, light is reflected by a *reflector* built into the cell. The reflective cell uses a single polarizer, which acts as in the parallel-polarizer configuration, as incident light after being reflected passes through it again (see Fig. 7). To obtain the same effect as the crossed-polarizer configuration, a quarter-wave film can be inserted beneath the polarizer.[25] It is also important to consider that in the case of a reflective cell, light has to propagate twice through the LC layer. For example, the total phase retardation will double for a reflective ECB cell,

$$\delta = 4\pi d\Delta n/\lambda, \tag{3}$$

compared to the same cell used in transmission.

Since different cells vary in their electro-optical properties due to the configuration and the materials used,[26,27] the cell design must be chosen depending on the application and required electro-optical characteristics. For experimental convenience, our first prototypes are based on reflective ECB cells.

III.C. Construction of the XLV

When constructing an XLV using *a*-Se, the biggest concern is the processing required: *a*-Se is particularly prone to damage from scratching involved in the processing steps, which can increase dark current due to injection from the surface, and heating above 60 °C, which can initiate recrystallization and consequent excessive dark current. The conventional method by which alignment layers are created involves rubbing and heating.[28] We have investigated several methods to reduce the opportunity for damage, including elimination of all processes involving heating. Very good results were obtained with photopolymerized alignment layers.[29] This also eliminates the potentially damaging rubbing process since alignment layers can be polymerized and

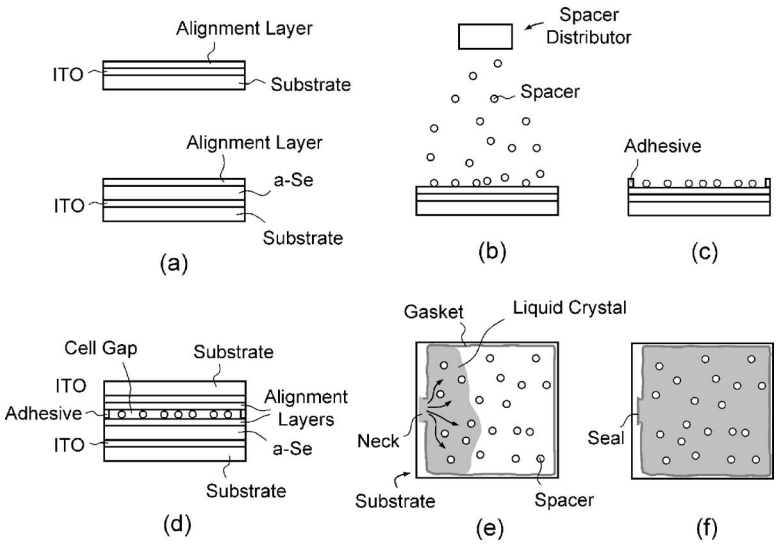

FIG. 8. Procedures to make a liquid crystal cell: (a) alignment layers are spin coated onto the surfaces, (b) the glass-only substrate is sprayed with spacers, (c) adhesive is placed around the perimeter to form a gasket, (d) both substrates are pressed together, (e) the LC mixture is added at the location of the neck and allowed to fill the gap by capillary action, and (f) the cell is sealed.

aligned in one step by irradiating with polarized UV light. Even the pre-tilt angle can be selected by changing the angle of incidence of the light.

The XLV should be constructed in a clean room. Figure 8 shows the main steps involved in making an XLV. First, two substrates are made of thin (0.5–1 mm) glass with a conductive and transparent indium tin oxide electrode. An *a*-Se layer (100–1000 μm) is evaporated onto one of the substrates. In the next step, very thin (10–50 nm) alignment layers are spin coated onto the surfaces which will enclose the LC [Fig. 8(a)]. They are polymerized and formed (i.e., a surface structure that will dictate the direction of alignment and the pre-tilt angle) by using linearly polarized UV light. The glass-only substrate is then placed in a spacer distributor and sprayed with spacers [Fig. 8(b)]. Afterwards, adhesive is placed around the perimeter [Fig. 8(c)] to form a gasket, allowing an opening (*neck*) for the LC to be added later. Both substrates are subsequently pressed together [Fig. 8(d)] and placed in a press to maintain the correct cell gap while the adhesive cures. The spacers keep a constant gap between both parts, which will later be filled with the LC mixture. The cured structure is placed in a vacuum chamber and then pumped down to about 30 mTorr. The LC mixture is added at the location of the neck using a vacuum manipulator and allowed to fill the gap by capillary action [Fig. 8(e)]. Once the cell is filled, it is taken out of the vacuum chamber and pressed again to establish contact between the spacers and the alignment layers, so ensuring the correct cell gap. While under pressure, it is sealed with epoxy [Fig. 8(f)], producing the finished XLV.

III.D. Digital readout

In order to keep the cost low, it is proposed to use a scanning approach for the readout so that it can be scaled to the number of pixels required for the application[19] without sacrificing resolution or pixel density. A scanning readout solves the problem of stitching images from more than one area CCD as discussed in Ref. 15. It is also much more convenient to make a readout system which operates solely from one side of the XLV. In order to do this, the XLV must be operated in reflective mode. The concept is shown in Fig. 9.

IV. RESULTS AND DISCUSSION

An XLV based on a reflective ECB cell was constructed and an example image demonstrating the basic feasibility of the concept is shown in Fig. 10. However, to be applicable in clinical radiography, the XLV must be sensitive enough to work within an appropriate range of diagnostic x-ray exposures. It must be x-ray quantum noise limited over this range and its resolution must be high.

IV.A. Characteristic curve and exposure range

In order to study the feasibility of the XLV for clinical imaging, mammography and chest radiography will be considered as examples of possible imaging tasks as they encompass the extremes of exposure levels and x-ray spectra

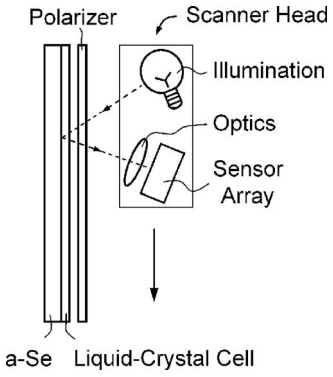

FIG. 9. Concept of scanner readout of an XLV operated in reflective mode. During the digitization of the optical image, the scanner head containing a light source and a linear array of sensors (with optics) is moved across the XLV as indicated by the arrow. A sheet polarizer is placed between the XLV and the scanner head. If necessary, the reflectivity of the XLV could be improved by adding a dielectric mirror between the *a*-Se and the LC cell.

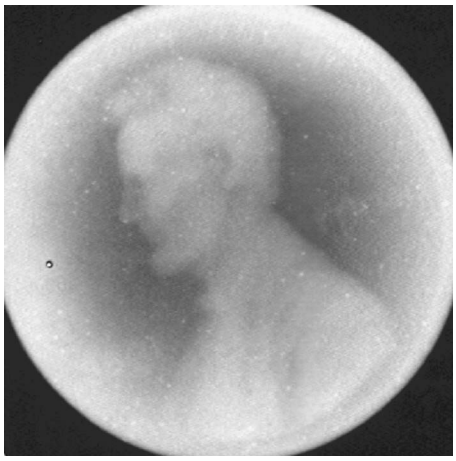

FIG. 10. Example x-ray image of a penny taken with our prototype (reflective ECB cell and 150 μm of *a*-Se) acquired at 60 kVp with an entrance exposure to the coin of ~27 mR (0.237 mGy). The image was corrected for structural noise by subtracting the preexposure image and multiplying by a gain matrix obtained from a flood field image.

required in diagnostic radiographic procedures. For these two applications, the means of clinical exposures expected at the detector are 0.3 mR for chest and 12 mR for mammography,[19] with an exposure range of 1/10–10 times the average exposure.

The x-ray sensitivity of a photoconductor depends on both the x-ray absorption, related to the atomic number and the thickness of the detector, as well as W, the energy required to release an ehp. For the two examples, one may consider 50 and 20 keV x rays, representing chest imaging and mammography, for which the linear attenuation coefficient, μ, of *a*-Se is 1.9×10^3 m^{-1} and 2.33×10^4 m^{-1}, respectively.[30] Thus 50% x-ray attenuation is achieved with a 365-μm-thick *a*-Se layer for a 50 keV beam and with a 30-μm-thick layer for a 20 keV beam. We have shown experimentally that the W of *a*-Se is a function of electric field, E.[31] At a typical bias electric field E of 10 V/μm, W is ~50 eV. The ratio of x-ray photon energy to W can be thought of as the quantum gain in the photoconductor. At 10 V/μm for *a*-Se, this gain is ~1000 ehp/(absorbed x ray) at 50 keV (diagnostic chest x-ray energy) and ~400 ehp/(absorbed x ray) at 20 keV (mammographic energy).

The LC cell should be sensitive to small changes in potential and these changes should result in a characteristic curve that is monotonic. The response time is not an issue for radiographic applications as in typical LC displays the molecules reach equilibrium in a tenth of a second or less.[32] However, the sensitivity is important since the XLV image charge, and thus the LC potential, is limited by the x-ray exposures that can be safely used in medical imaging. Linear response results in good contrast over a range of exposures. However, as long as the response is monotonic, it can be linearized. Typical LC cells require only a few volts across the LC layer in order to change from full blocking of light to full reflection. Figure 11(a) shows the relative reflectance of a reflective ECB cell as a function of potential, calculated by using the LC modeling software GNU-LCM.[33] The cell gap

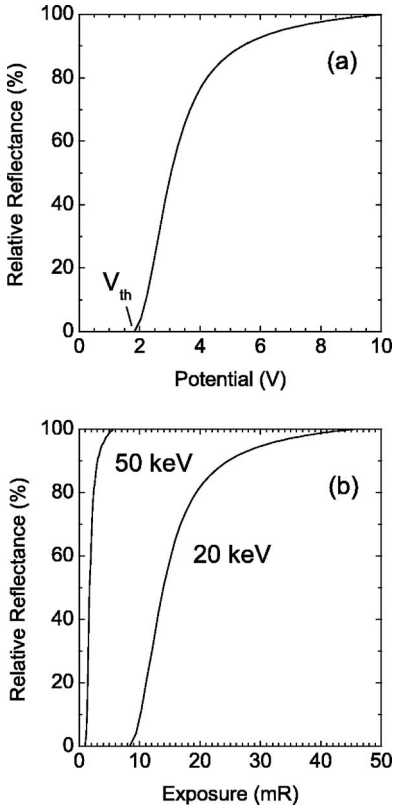

FIG. 11. The relative reflectance of a 1.7-μm-thick reflective ECB cell as a function of potential (a), calculated by using the liquid-crystal modeling software, can be combined with expected image charge based on a 500-μm-thick *a*-Se layer (at 10 V/μm) to obtain the relative reflectance as a function of exposure for 50 and 20 keV beams (b), representing chest radiography and mammography, respectively. The liquid-crystal cell is insensitive below a threshold voltage V_{th}=1.8 V.

of 1.7 μm was determined by using Eq. (3). The calculation is based on λ=640 nm and ZLI-4792, a LC mixture manufactured by Merck with the following properties: anisotropy in the index of refraction Δn=0.0969; dielectric constants of $\varepsilon_{\|}$=8.4 and $\varepsilon_{\perp}$=3.1.

In order to evaluate the performance of the XLV, it is critical to determine the relative reflectance change as a function of the amount of image charge collected on the surface of the *a*-Se, which in turn is proportional to the energy of the absorbed x-ray photons. The calculation assumes a monoenergetic beam, approximating the mean energy of commonly used spectra. The number of photons per Roentgen, N_R, for 50 keV and 20 keV beams, representing chest imaging and mammography, are 2.842×10^{14} m^{-2} and 5.493×10^{13} m^{-2}, respectively.[34] An exposure, X, of monoenergetic x rays gives rise to the image charge, Q, which can be expressed as

$$Q = X\eta N_{\mathrm{R}}(\xi/W)e, \tag{4}$$

where N_R is the number of photons per Roentgen, η is the quantum efficiency, ξ is the x-ray energy, and e is the electron charge. The magnitude of the signal potential across the LC can be calculated as a function using the above equation and the relationship

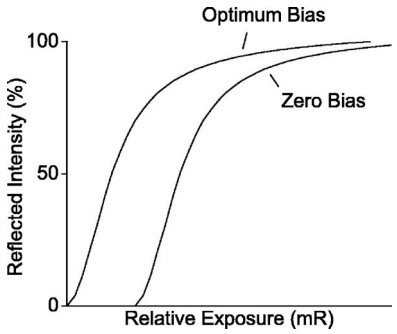

FIG. 12. Schematic showing how an electric field applied during the digitization step shifts the characteristic curve of the XLV to the left with respect to x-ray exposure. The external field adds to the field created by the image charge.

$$Q = CV, \tag{5}$$

where C is the capacitance of the cell and V is the potential.

Assuming that a 500-μm-thick a-Se layer (quantum efficiency of 62%) is used in a detector designed for chest radiography with a bias field of 10 V/μm, 1000 ehp are created per incident x-ray photon. By using Eqs. (4) and (5), and assuming that C is 1.6×10^{-5} F/m^2 (modeled by a parallel-plate capacitor), one obtains the relative reflectance as a function of exposure, which is shown in Fig. 11(b). The calculation is similar for mammography, where if the same detector is used, the quantum efficiency is 99.9% and 400 ehp will be created.

Since LC cells are insensitive below V_{th} (see Fig. 11), a small potential can be applied during the digitization step to bring the XLV to the threshold of its operating characteristics. The applied *readout bias* shifts the characteristic curve to the left with respect to x-ray exposure (see Fig. 12) because the external field adds to the field created by the image charge. Alternatively, actinic light emitted onto the photoconductor prior to the formation of an x-ray exposure can be used to bias the LC cell.[11]

Figure 13 shows that 0.3 mR incident on an XLV with a thick a-Se photoconductor will absorb most of the incident x rays and change the reflectance of the LC cell by a significant amount. This is adequate sensitivity for chest radiology. However, the predicted exposure range for mammography does not coincide with the clinical range. The higher mammographic exposures result in signal potentials across the LC layer which would saturate the LC cell. To better match the requirements for mammography, the signal handling capability of the XLV must be increased. One way to achieve this is to decrease the sensitivity by reducing the photoconductor quantum gain. Lower bias electric fields in the photoconductor during exposure will increase W, the energy required to produce an electron-hole pair, and thus decrease the gain (ξ/W), resulting in a greater exposure range for mammography. It should be noted that even if the sensitivity is decreased by reducing the photoconductor yield, there would still be many electron-hole pairs, namely (ξ/W), produced per absorbed x ray.

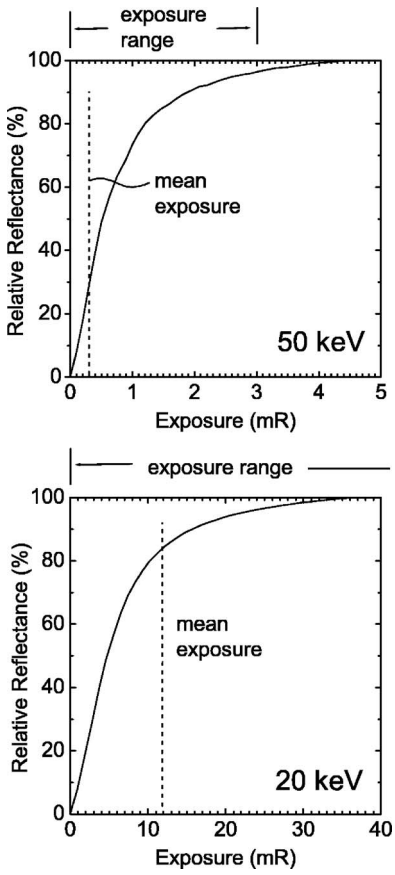

FIG. 13. The relative reflectance as a function of exposure of a XLV system biased during digitization for 50 keV (chest radiography) and 20 keV (mammography) beams. The calculation is based on a 500-μm-thick a-Se layer operated at 10 V/μm.

IV.B. Resolution

The spatial resolution is very high due to the high resolution of a-Se[35] and the thin LC cell (1.7 μm). Due to the very close proximity of the charge image to the LC cell, no significant loss of resolution due to electrostatic coupling occurs. Therefore, the resolution can be expected to be primarily limited by the pixel size of the readout system chosen.

Since the XLV is based on an electrostatic x-ray detector (a-Se), high image resolution can be achieved even with detectors thick enough to provide high quantum efficiency. In electrostatic detectors, the charge collection is guided by the presence of the electric field and there is very little resolution loss due to charge spread [Fig. 14(a)]. Instead, the inherent spatial resolution limit of a-Se is controlled by the x-ray interactions, namely the range of primary photoelectrons, reabsorption of characteristic radiation,[35] and in some cases trapping or recombination of charge in the a-Se layer. This makes a-Se a higher resolution detector than phosphors whose resolution limit (even in structured phosphors such as CsI) arise dominantly from optical spreading effects [Fig. 14(b)].[1]

Theoretically, the XLV concept has the potential to achieve very high image resolution, as demonstrated by ini-

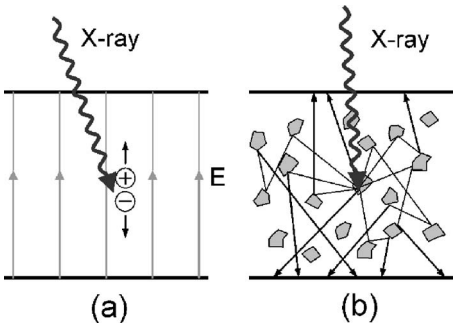

FIG. 14. Signal generation in an electrostatic detector (a) and a phosphor screen (b).

tial images. The resolution in some has been spectacular as shown in Fig. 15, an image demonstrating visualization of a 16.6 lp/mm lead bar pattern.

IV.C. Noise

The XLV noise sources can be separated in two types: *structural noise*, which arises from practical engineering limitations, and *fundamental noise*, which is due to physical limitations. Structural noise is caused by spatial variations in thicknesses and physical properties, or a non-uniform readout illumination. However, digital imaging acquisition should permit the correction of structural noise. A detailed study of the fundamental noise sources can be found elsewhere.[10] It is evident that the XLV has the potential to overcome electronic noise in the scanner because the amount of signal can be increased simply by increasing the external illumination level. Small and spatially uniform dark current in the photoconductor ensures that the dark current and its noise are negligible compared to the signal charge and its related noise. Provided that the *a*-Se/substrate interface forms a charge blocking contact, the *a*-Se dark current can be kept small at room temperature because of its large band-gap energy. The high sensitivity combined with negligible dark current and low structural noise ensures sufficient gain making it possible, in principle, to have an x-ray quantum limited system.

IV.D. Readout system

For the readout system, we propose the use of technology adapted from the familiar paper scanner that inputs documents and images into PCs. These devices have a retail cost in the US$100 range and, we believe, have adequate quality for this purpose. The most important reason that such modestly priced scanners can be used is that they are a consumer item and, therefore, the development and tooling costs have been amortized over millions of units, a volume that cannot be matched for devices designed for scientific or medical applications. Second, since unlimited light is available from the readout illumination, the sensitivity and noise required from the optical scanner are modest. The spatial resolution of scanner heads is remarkably high—600 dpi (*dots per inch*) (42.3 μm pixels) or 1200 dpi (21.2 μm pixels), and even 4800 dpi (5.3 μm pixels) are available. This is comparable to the pixel size used in AMFPIs designed for digital mammography (70–85 μm pixels). There are indications that the dynamic range of scanners is 16 bits internally though it is not yet known how many of these are useful. If as we anticipate 12 bits will be available, then the scanner can be used as it is.

The earlier images (Figs. 10 and 15) were acquired with a readout system based on a modified CanoScan LiDE 30 (Canon, Inc.) optical scanner, which is sold as an inexpensive paper scanner.

IV.E. Readout time

The optical image must be digitized before the charge stored in the *a*-Se-LC interface decays. This decay is a result of leakage currents through the LC and the *a*-Se, caused by mobile ions in the LC and charge injected in the photoconductor. However, the latter is known to be very small as, for example, in Xerography an image could be stored for tens of minutes before processing without significant loss of information. Therefore, an important requirement for the XLV is a sufficient time constant $\tau=RC$ of the LC layer, where R is the resistance of the mixture and C is the capacitance of the cell, which varies with the dielectric constant of the LC mixture used. Since the dielectric constant of the LC mixtures available for purchase only varies over a small range,[20] the

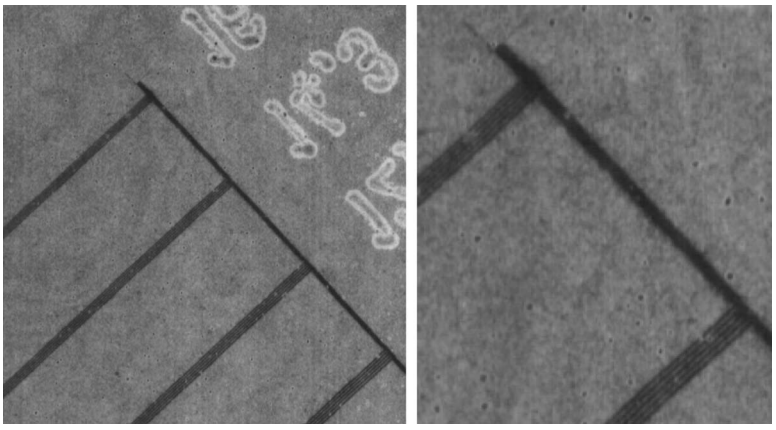

FIG. 15. Image of a lead bar pattern (Nuclear Associates, Carle Place, N.Y. 07-525, Nr 42145) showing 11.1, 12.5, 14.3, and 16.6 lp/mm, obtained using a prototype based on a reflective ECB cell and 150 μm of *a*-Se. The last two sections are shown magnified in the right pane for better visualization.

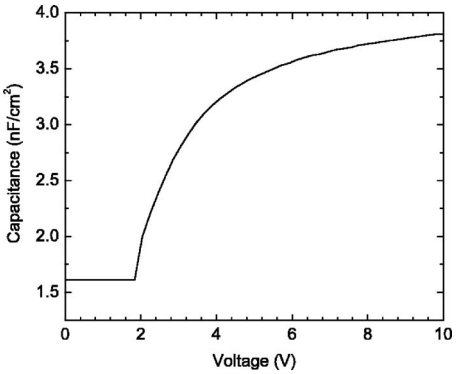

FIG. 16. The voltage dependent capacitance change of a 1.7-μm-thick ECB cell, calculated by using LC modeling software.

parameter which is used to achieve a long τ is the resistance. To maintain the image over a long time, carefully chosen high-resistivity or "high-holding" LC mixtures such as ZLI-4792 should be used.

IV.F. Capacitance

In Eq. (5), the capacitance of the cell was assumed constant, in which case the potential is proportional to the charge. However, LC cells exhibit a voltage dependent capacitance due to the anisotropic dielectric constant of the rod-shaped LC molecules. The applied potential causes the molecules to rotate, leading to a capacitance change.[36] This is illustrated in Fig. 16, which shows the voltage dependent capacitance change for a 1.7-μm-thick ECB cell, generated by using the software GNU-LCM.[33] It is apparent that we have a non-linear relationship between charge and reflection. In order to model our XLV more accurately, it will be necessary to measure this effect[37] and to consider it in future calculations.

IV.G. Different imaging tasks

Almost all key operating parameters depend on a number of adjustable variables, namely the electric field applied during exposure, the photoconductor gain, the acquisition time, and the electric field applied during digitization. Thus properties such as the operating characteristic can be adjusted for a desired imaging task by choosing the appropriate operating conditions and a single XLV unit may be used in diverse imaging tasks.

The ECB cell is not the only type of cell which can be used in an XLV. Different cells require different voltages to switch them. This fact can be used to accommodate various application requirements, for example, to design a detector optimized for portal imaging. In this case, the challenge results from the much higher x-ray energy and higher dose used compared to diagnostic imaging. Additionally, the imaging task in radiation therapy is not only to image the patient's anatomy with respect to the treatment portal (known as geometrical verification or portal imaging) but also to use the image to measure the dose delivered to the patient (known as dosimetric verification or exit dosimetry).

IV.H. X-ray damage

Since *a*-Se has a long history in medical x-ray imaging[17] and is currently used in AMFPIs,[1] its suitability for x-ray detectors is not under question. LC cells have also been shown to be practically immune to radiation damage up to at least 500 kGy, which is adequate for even radiation therapy applications.[38] Other elements such as the electronics and the optical imager can be shielded during exposure.

V. CONCLUSIONS

The XLV is essentially an image intensifier that can be used to construct an optically coupled digital radiographic system without a secondary quantum sink. Since the XLV is based on an electrostatic x-ray detector (*a*-Se), high image resolution can be achieved with detectors thick enough to provide high quantum efficiency. Thus the imaging chain of the XLV will be able to overcome all of the limitations typical of phosphor screen based digital imaging systems. In addition, since the XLV structure is simple, all elements are based on well-established technologies, and little external circuitry is required beyond a low profile optical scanner, the manufacturing costs could be kept significantly lower than competitive digital technologies. A properly optimized XLV would result in a versatile, inexpensive, high quality digital radiographic imaging system, and thus an attractive alternative for radiology departments globally.

ACKNOWLEDGMENT

We gratefully acknowledge financial support from the National Institutes of Health Grant No. 5-R01-EB-002-352-02, "Low cost digital x-ray detectors using liquid crystals."

[a]Author to whom correspondence should be addressed. Electronic mail: john.rowlands@sri.utoronto.ca

[1] J. A. Rowlands and J. Yorkston, *Medical Imaging. Volume 1 Physics and Psychophysics* (SPIE, Bellingham, 2000), pp. 223–328.
[2] W. Zhao, I. M. Blevis, D. F. Waechter, Z. Huang, and J. A. Rowlands, "Digital radiology using active matrix readout of amorphous selenium: Construction and evaluation of a prototype real-time detector," Med. Phys. **24**, 1834–1843 (1997).
[3] R. M. Nishikawa, G. E. Mawdsley, A. Fenster, and M. J. Yaffe, "Scanned-projection digital mammography," Med. Phys. **14**, 717–727 (1987).
[4] J. A. Rowlands, "Physics of computed radiography," Phys. Med. Biol. **47**, R123–R166 (2002).
[5] J. W. May and A. R. Lubinski, "High resolution computed radiography by scanned luminescent toner radiography," Proc. SPIE **1896**, 292–312 (1993).
[6] L. S. Jeromin and L. M. Klynn, "Electronic reading of x-ray images," J. Appl. Photogr. Eng. **5**, 183–189 (1979).
[7] U. Neitzel, I. Maack, and S. Gunther-Kohfahl, "Image quality of a digital chest radiography system based on a selenium detector," Med. Phys. **21**, 509–516 (1994).
[8] J. A. Rowlands and D. M. Hunter, "X-ray imaging using amorphous selenium: Photoinduced discharge (PID) readout for digital general radiography," Med. Phys. **22**, 1983–1996 (1995).
[9] M. Bath, P. Sund, and L. G. Mansson, "Evaluation of the imaging properties of two generations of a CCD-based system for digital chest radiography," Med. Phys. **29**, 2286–2297 (2002).
[10] P. K. Rieppo, B. Bahadur, and J. A. Rowlands, "Amorphous selenium liquid crystal light valve for x-ray imaging," Proc. SPIE **2432**, 228–236 (1995).
[11] P. K. Rieppo and J. A. Rowlands, "X-ray imaging using amorphous sele-

nium: Theoretical feasibility of the liquid crystal light valve for radiography," Med. Phys. **24**, 1279–1292 (1997).
[12]J. Grinberg, A. Jacobson, W. Bleha, L. Miller, L. Fraas, D. Boswell, and G. Myer, "A new real time non-coherent to coherent light image converter—The hybrid field effect liquid crystal light valve," Opt. Eng. (Bellingham) **14**, 217–225 (1975).
[13]D. Armitage, J. I. Thackara, and W. D. Eades, "Photoaddressed liquid crystal spatial light modulators," Appl. Opt. **28**, 4763–4771 (1989).
[14]J.-P. Huignard, S. LeBerre, C. Mayeux, and F. Micheron, "Liquid crystal image converter device," U.S. Patent No. 4,368,386, Jan. 11, 1983.
[15]M. J. Foley, P. W. Walton, W. van der Putten, and A. Workman, "Small area CCD based imaging system for use in digital mammography," in Proceedings of the 7th International Workshop on Digital Mammography (Durham, NC), pp. 37–45 (unpublished).
[16]M. J. Foley, P. W. Walton, and W. van der Putten, "Development of an image receptor for use in Digital mammography," Proc. SPIE **4876**, 54–60 (2003).
[17]J. W. Boag, "Xeroradiography," Phys. Med. Biol. **18**, 3–37 (1973).
[18]J. Mort, *The Anatomy of Xerography: Its Invention and Evolution* (McFarland, London, 1989).
[19]W. Zhao and J. A. Rowlands, "X-ray imaging using amorphous selenium: Feasibility of a flat panel self-scanned detector for digital radiology," Med. Phys. **22**, 1595–1604 (1995).
[20]*Liquid Crystal Mixtures For Electro-Optical Displays* (Merck Ltd./BDH, 1992).
[21]M. Schadt and W. Helfrich, "Voltage-dependent optical activity of a twisted nematic liquid crystal," Appl. Phys. Lett. **18**, 127–128 (1971).
[22]M. Born and E. Wolf, *Principles of Optics* (Pergamon, New York, 1980).
[23]S. T. Wu and C. S. Wu, "Mixed-mode twisted nematic cells for reflective liquid crystal displays," Appl. Phys. Lett. **68**, 1455–1457 (1996).
[24]P. Yeh and C. Gu, *Optics of Liquid Crystal Displays* (Wiley, New York, 1999).
[25]S. T. Wu and D. K. Yang, *Reflective Liquid Crystal Displays* (Wiley, New York, 2005).
[26]B. Bahadur, *Molecular Crystals and Liquid Crystals-Special Topics X*, edited by G. J. Dienes, M. M. Labes, and G. H. Brown (Gordon and Breach, New York, 1984), pp. 47–49, 81.
[27]B. Bahadur, Ed., *Liquid Crystals-Applications and Uses, Vol. 1* (World Scientific, 1990), pp. 239–240.
[28]W. C. O'Mara, *Liquid Crystal Flat Panel Displays: Manufacturing Science & Technology* (Chapman and Hall, New York, 1993).
[29]M. Schadt, H. Seiberle, A. Schuster, and S. M. Kelly, "Photo-generation of linearly polymerized liquid crystal aligning layers comprising novel, integrated optically patterned retarders and color filters," Jpn. J. Appl. Phys., Part 1 **34**, 3240–3249 (1995).
[30]E. F. Plechaty, D. E. Cullen, and R. J. Howerton, *Tables and Graphs of Photon Interaction Cross Sections from 1.0 keV to 100 MeV Derived from LLL Evaluated Nuclear Data Library. UCRL-50400 Vol. 6 Revision 1* (University of California Lawrence Livermore Laboratory, Springfield, 1975; National Technical Information Service, 1975).
[31]I. M. Blevis, D. C. Hunt, and J. A. Rowlands, "Measurement of x-ray photogeneration in amorphous selenium," J. Appl. Phys. **85**, 7958–7963 (1999).
[32]P. Collings, *Liquid Crystals, Nature's Delicate Phase of Matter* (Princeton University Press, Princeton, 1990).
[33]GNU-LCM was developed by Salman Saeed, BOSLab Research Group, Liquid Crystal Institute, Kent State University, Kent, Ohio, USA under funding from NATO. It uses the Birefringent Thin Films Toolbox developed by and copyright I. J. Hodgkinson and Q. Wu, of the University of Otago, Dunedin, Otago, New Zealand.
[34]H. E. Johns and J. R. Cunningham, *The Physics of Radiology* (Charles C. Thomas, Springfield, 1983), p. 722.
[35]W. Que and J. A. Rowlands, "X-ray imaging using amorphous selenium: Inherent spatial resolution," Med. Phys. **22**, 365–374 (1995).
[36]P. Photinos, *Liquid Crystals, Experimental Study of Physical Properties and Phase Transitions*, edited by S. Kumar (Cambridge University Press, Cambridge, 2001) pp. 95–151.
[37]K. C. Schad, I. Koprinarov, C. A. Webster, and J. A. Rowlands, "The x-ray light valve-prediction of the x-ray characteristic curve and its application to liquid-crystal-cell design," Med. Phys. (submitted).
[38]D. M. Korn, S. P. Johnson, O. L. Nelson, and R. J. Ziegler, "A method of electronic readout of electrophotographic and electroradiographic images," J. Appl. Photogr. Eng. **4**, 178–182 (1978).